# Generation of intense proton beams from plastic targets irradiated by an ultraintense laser pulse

K. Lee,[1,*] S. H. Park,[1] Y.-H. Cha,[1] J. Y. Lee,[1,2] Y. W. Lee,[1,3] K.-H. Yea,[1] and Y. U. Jeong[1]
[1]*Quantum Optics Center, Korea Atomic Energy Research Institute, Daejeon 305-353, Korea*
[2]*Department of Applied Optics and Electromagnetics, Hannam University, Daejeon 306-791, Korea*
[3]*Department of Physics, Yeungnam University, Gyeongbuk 712-749, Korea*
(Received 20 October 2007; revised manuscript received 6 September 2008; published 10 November 2008)

Proton beams generated from thin aluminum and Mylar foil targets that are irradiated by a 30 fs Ti:sapphire laser pulse with an intensity of $2.2\times10^{18}$ W/cm$^2$ were investigated. Protons from the Mylar targets were observed to have an energy higher by a factor of 2 and were higher in number by an order of magnitude as compared with those generated from the aluminum targets. The maximum proton energy of $1.3\pm0.12$ MeV obtained from the Mylar target was found to be similar with previous observations that used laser pulses with different intensities. To address the anomalous behavior of the maximum proton energy for plastic targets, an acceleration model is proposed. In this model, the protons are accelerated by a resistively induced electric field in the front of the target, which can account for the experimental observations.

DOI: 10.1103/PhysRevE.78.056403 PACS number(s): 52.38.Kd, 52.50.Jm

## I. INTRODUCTION

Energetic ion beams are generated by irradiating thin foil targets with an ultraintense laser pulse [1]. The proton beams are found to possess high beam quality [2], short pulse duration, and stable beam pointing [3]. The possibilities of a monoenergetic beam were also demonstrated for both protons [4] and carbon ions [5]. These characteristics have enabled the application of the laser-accelerated ion beams to various fields [6] such as radioisotope generation, proton radiography of plasma, fast ignition for inertial fusion, cancer therapy, and nuclear physics.

There has been a long-standing controversy on the origin of the accelerated protons; recently, Fuchs *et al.* [7,8] have shown that in the case of metal targets, rear-side acceleration is dominant. In addition, there is another issue concerning the target materials that has to be resolved. Fritzler *et al.* [9] obtained a higher number of protons from aluminum targets as compared with that obtained from Mylar targets, but with similar maximum energies. In contrast, other experimental results show that plastic targets generate protons whose energies and numbers are higher than those of metal targets [10–12]. Metal foil targets coated with thin plastic have shown considerable increase in the energy and number of protons as compared with the uncoated metal foil targets [13,14]. These circumstances motivated the authors to investigate laser-accelerated proton beams generated from plastic targets.

In this paper, we present laser-accelerated proton beams from aluminum and Mylar targets with different thicknesses irradiated by a laser pulse with an intensity of $2.2\times10^{18}$ W/cm$^2$ and a pulse width of 30 fs. The energy spectra show that the protons from the Mylar target have a higher maximum energy and higher number, which is similar to the observations [11,12]. The maximum proton energy of 1.3 MeV was observed from a 13-$\mu$m-thick Mylar target and it is similar to 1.5 MeV [11] and 1.2 MeV [12], even though the laser intensity in the present study is much different from those in these references. A comparison of the maximum energies of protons generated from Mylar targets with an isothermal expansion model [7,8,15] shows that there are large discrepancies in the intensity range of $10^{17}$–$10^{19}$ W/cm$^2$. To account for the anomalous behavior of the maximum proton energy for Mylar targets, we propose an acceleration model involving a strong electric field in the front side of the target induced by the resistivity of a background cold plasma [16], and the estimations of maximum proton energies by the model show that it effectively predicts the experimental observations in the laser intensity range of $10^{17}$–$10^{19}$ W/cm$^2$ for Mylar targets.

## II. EXPERIMENTAL SETUP

Experiments have been conducted by using a 10 TW Ti:sapphire laser developed at the Korea Atomic Energy Research Institute (KAERI); the laser can deliver up to 300 mJ of energy with a pulse width of 30 fs at a central wavelength of 0.8 $\mu$m. The beam has $p$ polarization and is focused on a target at an incident angle of 45° by using an $f/4.5$ off-axis parabola mirror. The full-width-half-maximum of the focal size in laser intensity was measured to be 12 $\mu$m. The contrast ratio of the amplified spontaneous emission (ASE) at 10 ns was estimated to be $10^{-8}$ [17]. The proton beams generated by irradiating thin foil targets with the laser pulse were measured using a Thomson parabola spectrometer (TPS) and a Faraday cup (FC). The TPS was installed to measure the proton energy spectrum in the forward direction normal to the target surface and 32 cm away from the target. It was equipped with a CR39 plastic nuclear track detector [18]. A pinhole with a diameter of 400 $\mu$m was installed in front of the TPS, and the corresponding solid angle was $1.2\times10^{-6}$ sr.

## III. EXPERIMENTAL RESULTS

For target materials, aluminum foils with thicknesses of 2, 6, 15, 18, and 50 $\mu$m and Mylar foils with thicknesses of 1.5,

*klee@kaeri.re.kr

 

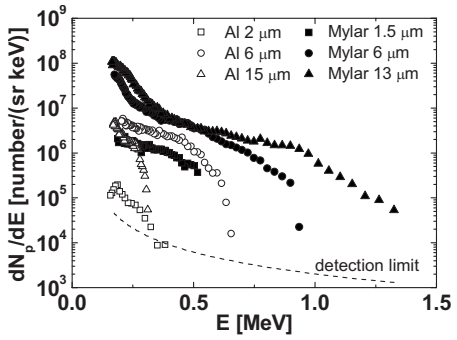


FIG. 1. Proton energy spectra generated from aluminum and Mylar targets are plotted; it is observed that protons from the Mylar targets are higher in number and energy. Targets with a thickness of 50 $\mu$m are also used, resulting in the absence of protons for the aluminum target and protons with energies lower than 0.2 MeV for the Mylar target. The dotted line indicates the detection limit of the TPS.

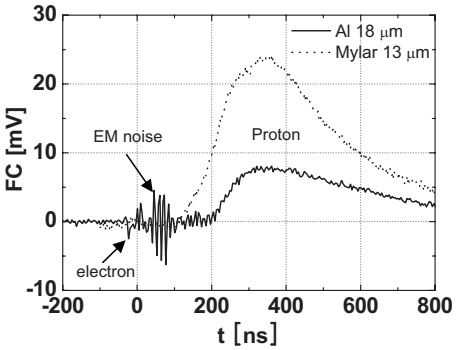


FIG. 2. Typical FC signals for the 18-$\mu$m-thick aluminum target and the 13-$\mu$m-thick Mylar target are plotted; these signals also show that protons from the Mylar target are higher in number (stronger signal) and energy (faster rise). An electron signal can be clearly observed for the aluminum target, but no such signal is observed for the Mylar target.

6, 13, and 50 $\mu$m were used to investigate the proton beams generated from metal and plastic materials. In this experiment, a laser energy of 230 mJ was used, which amounts to $2.2\times10^{18}$ W/cm$^2$ in intensity with approximately 50% of the laser energy being in the focal area. This intensity corresponds to the normalized vector potential $a=0.85\times\lambda I^{1/2}\simeq1$, where $\lambda$ is the wavelength in $\mu$m and $I$ is the intensity in $10^{18}$ W/cm$^2$.

Figure 1 shows the proton energy spectra obtained using the TPS for the aluminum and Mylar targets. Due to shot-to-shot variations, data were accumulated over 10–16 shots for each spectrum. In the case of the 50-$\mu$m-thick aluminum target, no protons were obtained, and only protons with energies less than 0.2 MeV were obtained for the 50-$\mu$m-thick Mylar target. The amount of protons generated from the Mylar targets is significantly larger than that generated from aluminum targets, which is similar to previous observations [11,12]. A maximum proton energy of $1.3\pm0.12$ MeV is obtained for a 13-$\mu$m-thick Mylar target, which is two times higher than the energy of $0.65\pm0.04$ MeV obtained for a 6-$\mu$m-thick aluminum target. This tendency on target materials can also be observed in the FC signals plotted in Fig. 2, which shows the proton signal rising faster and higher in the case of the Mylar target as compared with the case of the aluminum target.

It is very interesting to note that in the case of the Mylar target, the maximum proton energy of 1.3 MeV is similar to the values in the previous observations, 1.2 MeV [12] and 1.5 MeV [11], even though these values were obtained with laser intensities that were lower by 8.8 times and higher by 3.2 times, respectively, as compared to the intensity in our study. There are some observations that indicate the laser prepulse influences on the maximum energy [19,20]. However, since the maximum proton energies for the aluminum targets vary from 0.2 to 0.95 MeV and since they are found to be well predicted by the isothermal expansion model (see below), the effect of different prepulse conditions on this anomalous behavior of the maximum energy for the Mylar target could be neglected.

In order to observe the anomalous behavior of the maximum proton energy for the Mylar target, previous experimental observations have been investigated, which shows interesting behaviors with regard to the laser intensities for different target materials. In Fig. 3, maximum proton energies taken from Refs. [3,9,11–14,21] are plotted against the laser intensity; our values are also plotted. It is well known that a laser pulse with a longer pulse width but constant intensity produces higher-energy protons. Thus, data that involved the use of ultrashort pulse lasers with pulse width of 30–100 fs are selected to clearly observe the behavior of the maximum proton energy against the laser intensity. A clear difference is observed between the aluminum and Mylar targets. It is also interesting to note that the maximum proton energies for metal targets coated with plastic are placed between those for the metal and Mylar targets. The experimental data are compared with the predictions of the isothermal expansion model [7,8,15] or target normal sheath acceleration (TNSA) model. In this model, the ions are accelerated by the sheath field built at the rear side of the target by hot electrons, which are accelerated by the ponderomotive force

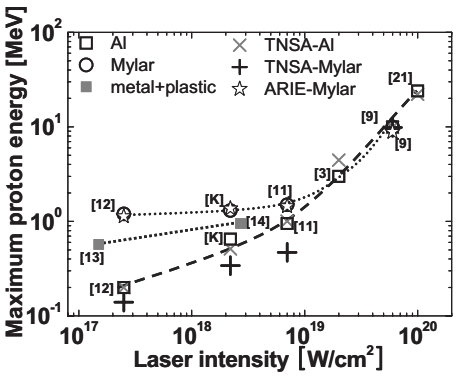


FIG. 3. Maximum proton energies are plotted against the laser intensity. The numbers in the symbol represent numbers of the references from which the data are obtained, and current results are designated by "K." The theoretical estimations obtained from the isothermal expansion model (TNSA) ($\times$ for aluminum and $+$ for Mylar) and by the ARIE model for Mylar ($\star$) are also plotted. For the data points designated by Ref. [9], all the experimental and theoretical points are overlapped. Lines are added for a better view.

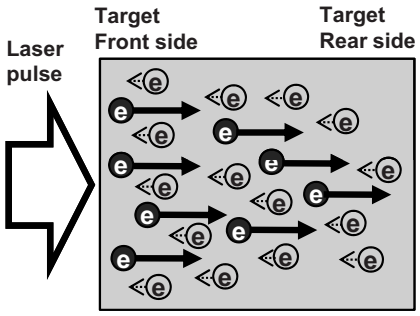


FIG. 4. This shows that return current by the electrons in a background plasma (open circles with small arrows) balances the very high current by the hot electrons (filled circles with large arrows), which is accelerated by the laser pulse at the front side of the target. When the resistivity of the background plasma cannot be neglected, a strong electrostatic field can be set at the front side of the target, which inhibits the transport of the hot electrons and accelerates protons in the acceleration by a resistively induced electric field (ARIE) model proposed in the current paper.

of the laser field at the front side and transported through the target. We can observe that there are large discrepancies in the maximum proton energies for the Mylar target between the predictions of the TNSA model (+) and the experimental results (○) for the laser intensity range of $10^{17}-10^{19}$ W/cm$^2$, while in the case of the aluminum target, the agreement is good. The discrepancy increases as the laser intensity decreases.

## IV. ACCELERATION BY A RESISTIVELY INDUCED ELECTRIC FIELD: MODEL

These investigations of the different behaviors of maximum proton energies between the Mylar and aluminum targets—considerably high proton energy for the Mylar target, its weak dependence on the laser intensity, and failure of the TNSA model at low intensities—suggest that in order to properly treat an acceleration mechanism for the plastic target, the model should include some material properties. Recently, Gibbon [22] performed a three-dimensional particle-in-cell simulation with the inclusion of a collisional transport effect in a self-consistent manner and showed that the front-side acceleration becomes dominant and enhanced with an increase in the target resistivity. Observations do exist for insulator targets, and they indicate that the transport of hot electrons is inhibited by the resistively induced electric field (RIE) [23,24]. In the FC measurement, the electron signals from the aluminum target were clearly observed, whereas no such signals appeared from the Mylar target (Fig. 2). This may be related to the inhibition of hot electron transport inside the Mylar target.

This phenomenon was analytically investigated by Bell *et al.* [16]. They considered a balancing return current $J_{\mathrm{return}}$ by background cold electrons to support the very high current $J_{\mathrm{hot}}$ resulting from ponderomotively-accelerated hot electrons, i.e., $J_{\mathrm{return}}+J_{\mathrm{hot}}\simeq 0$, as shown in Fig. 4. If the resistivity of the background plasma $\eta$ is negligible, the return current readily neutralizes the charge separation set by the hot electrons. Thus the hot electrons can transport through the target reaching at the rear side of the target. However, if it cannot be neglected, according to the ohmic relation $E_r = \eta J_{\mathrm{return}}$, an electric field called RIE can be set in the front side of the target, which inhibits the transport of the hot electrons.

Based on the analysis of Bell *et al.*, we propose an acceleration model, which can address the anomalous behavior of maximum proton energies for the Mylar target at low laser intensities. We used most of the analytical results from Ref. [16]. But in the derivation of $E_r$, to avoid an indefinite increase of the hot electron velocity $v_h$ over the speed of light as $\eta$ increases, we used $J_{\mathrm{hot}}\simeq -n_h e v_h$ instead of using the speed of light for the hot electron velocity as done in Ref. [16]. The hot electron velocity was obtained by using the ponderomotive potential or the hot electron temperature $T_h = m_e c^2(\sqrt{1+a^2}-1)$ [15]. Then, the RIE at the end of the laser pulse is obtained as

$$E_r = E_o\left(\frac{x_o}{x+x_o}\right)^2, \tag{1}$$

where $x$ is the distance from the front surface of the target and $E_o = ecn_{ho}\eta a/\sqrt{1+a^2}$. The hot electron density at $x=0$ ($n_{ho}$) and the penetration depth ($x_o$) can be written in convenient forms as follows [16]:

$$n_{ho} = 1.4\times 10^{20}\frac{\eta f^2 I^2 \tau_L}{T_h^3}\ \mathrm{cm}^{-3}, \tag{2}$$

$$x_o = 300\frac{T_h^2}{\eta f I}\ \mu\mathrm{m}, \tag{3}$$

where $f$ is the absorption efficiency of the laser energy into the hot electron, $I$ is the laser intensity in $10^{18}$ W/cm$^2$, and $\tau_L$ is the laser pulse width in ps. $T_h$ and $\eta$ are expressed in units of MeV and $\mu\Omega$ m, respectively. Assuming a static condition, the maximum energy acquired by the protons in the RIE can be expressed as $E_p^{\max} = eE_o x_o$. This can be written as follows:

$$E_p^{max} \simeq 2\frac{\eta f I \tau_L}{T_h}\frac{a}{\sqrt{1+a^2}}\ \mathrm{MeV}. \tag{4}$$

This formula for the acceleration by a resistively induced electric field (ARIE) includes the resistivity of the background cold plasma. From the measurement of hot electron transport, Pisani *et al.* [23] inferred that in the plastic targets, the plasma has a higher resistivity as compared to that in the metal targets. When the background resistivity is high or the penetration depth is considerably smaller than the target thickness, the ARIE can be dominant; such a situation can be expected to occur in insulator targets. This acceleration mechanism can also be considered as a bulk acceleration, which accounts for the higher number of protons from the Mylar targets. The maximum proton energies estimated by using the ARIE model are plotted in Fig. 3 for the Mylar targets (⋆), and this shows that the model can account for the experimental observations. The parameters used to evaluate the maximum proton energies for Mylar targets are listed in

TABLE I. The parameters used to evaluate theoretical estimations are listed. $d$ is the target thickness. The absorption efficiencies, $f$ were obtained from Ref. [25] for two low laser intensities and from Ref. [7] for two high laser intensities. The plasma resistivity were selected to reproduce the experimental results. The reference designated by "K" is current result.

| I ($W/cm^2$) | $\tau_L$ (fs) | $d$ ($\mu$m) | $f$ (%) | $T_h$ (MeV) | $\eta$ ($\mu\Omega$ m) | $n_{ho}$ ($cm^{-3}$) | $x_o$ ($\mu$m) | $E_o$ (V/cm) | $E_p^{max}$ (MeV) ARIE | TNSA | EXP |
|---|---|---|---|---|---|---|---|---|---|---|---|
| $2.5\times10^{17}$ | 40 | 2.5 | 5 | 0.029 | 100 | $3.7\times10^{21}$ | 0.20 | $5.7\times10^{10}$ | 1.1 | 0.14 | 1.2 [12] |
| $2.2\times10^{18}$ | 30 | 13 | 5 | 0.21 | 60 | $3.5\times10^{20}$ | 1.9 | $7.1\times10^{9}$ | 1.4 | 0.34 | 1.3 [K] |
| $7\times10^{18}$ | 60 | 23 | 11 | 0.54 | 10 | $2.9\times10^{20}$ | 12 | $1.2\times10^{9}$ | 1.4 | 0.47 | 1.5 [11] |
| $6\times10^{19}$ | 40 | 6 | 52 | 2.2 | 8 | $3.9\times10^{21}$ | 6.0 | $1.5\times10^{10}$ | 8.9 | 10 | 10 [9] |

Table I. In these estimations, since it is difficult to determine the background plasma resistivity in a self-consistent manner, this parameter can be considered to be strongly related to the laser prepulse and target materials; the plasma resistivities were selected to reproduce the experimental values. The high values of $\eta$ at low laser intensities can be understood from the low prepulse intensities at low laser intensities. These values can also be considered to be reasonable since they are considerably higher at low laser intensity than the measured resistivity of an aluminum plasma, i.e., 2 $\mu\Omega$ m [26]. In the case of the data obtained from Ref. [9], even though the ARIE model reproduces the experimental maximum proton energy, the TNSA mechanism can be considered as the main acceleration mechanism from the observation of higher numbers of protons from the aluminum target as compared to that from the Mylar target. The penetration depth is also estimated to be similar with the target thickness of 6 $\mu$m, which implies that the hot electrons can reach the rear side of the target to build the sheath in the TNSA model.

## V. SUMMARY

Laser-accelerated proton beams from aluminum and Mylar targets irradiated by an ultrashort laser pulse were investigated. The observed proton energy spectra show that the Mylar target generates a considerably higher number of protons as compared to the aluminum target by an order of magnitude and the maximum proton energy of the former target is higher than the latter target by a factor of 2. The maximum proton energies obtained from various experimental observations are compared with the predictions of the isothermal expansion model, and large discrepancies are observed for the Mylar target at laser intensities of $10^{17}$–$10^{19}$ $W/cm^2$. Based on the analysis of Bell *et al.* [16], an acceleration model (ARIE) is proposed; this model is effective in explaining the anomalous behavior of the maximum proton energy for the Mylar target at low laser intensities. With appropriate choices of the background plasma resistivity, it also reproduces experimental results, even though it requires a more refined analysis for the background plasma resistivity.


[1] M. D. Perry and G. Mourou, Science **264**, 917 (1994).
[2] T. E. Cowan *et al.*, Phys. Rev. Lett. **92**, 204801 (2004).
[3] J. Schreiber *et al.*, Phys. Plasmas **13**, 033111 (2006).
[4] H. Schwoerer *et al.*, Nature (London) **439**, 445 (2006).
[5] B. M. Hegelich *et al.*, Nature (London) **439**, 441 (2006).
[6] D. Umstadter, J. Phys. D **36**, R151 (2003).
[7] J. Fuchs *et al.*, Nat. Phys. **2**, 48 (2006).
[8] J. Fuchs *et al.*, Phys. Plasmas **14**, 053105 (2007).
[9] S. Fritzler *et al.*, Appl. Phys. Lett. **83**, 3039 (2003).
[10] R. A. Snavely *et al.*, Phys. Rev. Lett. **85**, 2945 (2000).
[11] I. Spencer *et al.*, Phys. Rev. E **67**, 046402 (2003).
[12] Y. Wada, Jpn. J. Appl. Phys., Part 1 **44**, 3299 (2005).
[13] H. Kishimura *et al.*, Appl. Phys. Lett. **85**, 2736 (2004).
[14] A. Yogo *et al.*, Appl. Phys. B: Lasers Opt. **83**, 487 (2006).
[15] P. Mora, Phys. Rev. Lett. **90**, 185002 (2003).
[16] A. R. Bell *et al.*, Plasma Phys. Controlled Fusion **39**, 653 (1997).
[17] Y. H. Cha *et al.*, Appl. Opt. **46**, 6854 (2007).
[18] J. Y. Lee *et al.*, J. Korean Phys. Soc. **51**, 426 (2007).
[19] M. Kaluza, J. Schreiber, M. I. K. Santala, G. D. Tsakiris, K. Eidmann, J. Meyer-ter-Vehn, and K. J. Witte, Phys. Rev. Lett. **93**, 045003 (2004).
[20] H. J. Lee *et al.*, Phys. Plasmas **11**, 1726 (2004).
[21] A. J. Mackinnon, Y. Sentoku, P. K. Patel, D. W. Price, S. Hatchett, M. H. Key, C. Andersen, R. Snavely, and R. R. Freeman, Phys. Rev. Lett. **88**, 215006 (2002).
[22] P. Gibbon, Phys. Rev. E **72**, 026411 (2005).
[23] F. Pisani *et al.*, Phys. Rev. E **62**, R5927 (2000).
[24] D. Batani *et al.*, Phys. Rev. E **65**, 066409 (2002).
[25] D. F. Price, R. M. More, R. S. Walling, G. Guethlein, R. L. Shepherd, R. E. Stewart, and W. E. White, Phys. Rev. Lett. **75**, 252 (1995).
[26] H. M. Milchberg, R. R. Freeman, S. C. Davey, and R. M. More, Phys. Rev. Lett. **61**, 2364 (1988).